Calculation of near K edge x-ray absorption spectra and hydrogen bond network in ice XIII under compression

ARTICLE *in* THE JOURNAL OF CHEMICAL PHYSICS · MAY 2010

Impact Factor: 2.95 · DOI: 10.1063/1.3421650

3 AUTHORS, INCLUDING:

Z. R. Xiao
Taiwan Semiconductor Manufacturing
19 PUBLICATIONS **248** CITATIONS

Calculation of near *K* edge x-ray absorption spectra and hydrogen bond network in ice XIII under compression

Jingyun Zhang,[1] Zhi-Ren Xiao,[2] and Jer-Lai Kuo[1,3,a)]
[1]*School of Physical and Mathematical Sciences, Nanyang Technological University, Singapore 637371*
[2]*Center for General Education, National Taiwan Normal University, Taipei 10610, Taiwan*
[3]*Institute of Atomic and Molecular Sciences, Academia Sinica, Taipei 10617, Taiwan*

(Received 8 December 2009; accepted 12 April 2010; published online 12 May 2010)

The hydrogen bond network, oxygen *K* edge x-ray absorption spectra (XAS), and electronic structure of ice XIII under compression have been extensively studied by density functional theory (DFT). We showed that DFT methods yield a ground state consistent with previous neutron scattering experiment and a few low-enthalpy metastable states are likely to coexist from the total enthalpy calculations. Oxygen *K* edge XAS of four low-enthalpy configurations was studied with the aim to shed light on the local structure in these configurations. We demonstrated that pre-edge of oxygen *K* edge XAS is a common feature appearing in all these four structures while major spectral differences exist in the main peak area. Therefore, we arrived at the conclusion that the main peak is more sensitive to the local hydrogen bond environment and could be used as an effective tool to distinguish these four configurations. We also found that the pre-edge has main contribution from O $1s$-$4a_1$ transitions and its intensity was suppressed by pressure while the main peak is mostly coming from O $1s$-$2b_2$ transitions. © *2010 American Institute of Physics*. [doi:10.1063/1.3421650]

I. INTRODUCTION

Ice has an intricate phase diagram with at least 15 crystalline phases identified experimentally until now. Very recently, two new phases were found by Salzmann *et al.*[1] and they were labeled as ice XIII and ice XIV, respectively. Experimental challenges associated with low temperatures/slow kinetics, low scattering power of protons, and difficulties in locating precise phase boundaries all conspire to make comparisons among experiments nontrivial. On the theoretical side, much has been learned about ice physics by means of empirical models[2,3] and more recently, there is a growing trend on the application of first principles methods.[4,5] In all the known crystalline phases of ice, oxygen atoms must have tetrahedral coordination, but the hydrogen atoms may be disordered or ordered subject to the constraint of "ice rules."[6] In spite of these restrictions, a very large number of nearly degenerate molecular configurations, which are all related to each other by cooperative reorientation, exist near the true ground state. Although a number of empirical potential models[3,7] were able to reproduce the complex features of the water phase diagram, the relative stability of proton disordered and ordered phases are usually predicted incorrectly.[8] Instead of using an empirical model, very recently, the structure prediction of ice XIV was reported by Tribello *et al.*[4] based on density functional theory (DFT) calculations and they suggested two or more metastable, proton ordered structures of ice XIV.

According to the powder neutron diffraction,[1] ice XIII, the proton-ordered counterpart of ice V, has a primitive monoclinic cell comprising 28 molecules with seven crystallographically distinct oxygen atoms. The highest symmetry space group of ice XIII from the observed reflection condition is monoclinic $P2_1/a$, which is a subgroup of the ice V space group (A2/a) making ice XIII the most complicated structure among all the known crystalline structures. Knight and Singer[9] studied hydrogen bond fluctuations and proton ordering thermodynamics in ice V and XIII with statistical mechanical techniques focusing on the phase transition along the temperature scale. In this work, we are motivated to investigate the pressure influences on the electronic structure and bonding properties. Here, we employed all possible ice-rule-allowed configurations enumeration scheme,[10] which has been successfully applied to ice Ih,[11] ice VII/VIII,[12] and ice VI (Ref. 13) in our previous works. We found that the experimentally proposed fully ordered structure is energetically competitive in this work due to the fact that it is one of the lowest enthalpy structures of the given ice XIII phase identified by DFT.

Recently, core level spectroscopy has been shown to be a powerful tool to probe local structure and the main advantage of x-ray absorption spectroscopy (XAS) is its ability to selectively excite individual atom and thereby examine the specific chemical environment around the excited atom.[14] This newly emerging technique has recently been applied to liquid and other condensed phases of water, in which a surprising sensitivity of the electronic structure to the coordination and bonding situation has been proposed.[15–18] In combinations with electronic structure calculations, the pre-edge feature and the main-edge of the oxygen *K* edge XAS were identified to be associated with water molecules with broken hydrogen bonds, whereas the post-edge region was mainly

a)Author to whom correspondence should be addressed. Electronic mail: jlkuo@pub.iams.sinica.edu.tw.

related to fully coordinated molecules.[16,18–20] These studies have the potential to provide crucial information on the hydrogen bonding characters in liquid water on the subfemtosecond time scale. In Sec. III, we report our calculations on the oxygen *K* edge XAS of four metastable states to examine the sensitivity of application of oxygen *K* edge XAS to distinguish local hydrogen bond network. Meanwhile, we analyze the origin of the oxygen *K* edge XAS spectral features through analysis of the partial density of states (DOS) of oxygen atoms. Furthermore, we also carried out a close examination of the effects of pressure on oxygen *K* edge XAS and covalent OH bond.

II. COMPUTATION METHODS

We started by exploring all the possible hydrogen-bonding configurations for ice XIII allowed by the ice rule in a unit cell of 28 water molecules. Due to the size and low symmetry of the ice XIII unit cell, application of the methodology results in enumeration of 69 380 symmetry-distinct hydrogen-bonding configurations. This complexity makes the prediction of the proton ordered phase and the analysis of its properties challenging and formidable. To reduce the number of structures for following optimization calculations and since it has been speculated that the proton ordered phase should have maximal symmetry,[4] we only consider the high symmetry configurations. Therefore, only 70 structures are selected for following enthalpy calculations; these structures fall into two main groups classified by different space group of $P2_1/a$ and CC. Each structure was fully relaxed and the relative enthalpies[4] (H=E+PV) were calculated using the plane wave code VASP.[21] We adopted the projector-augmented wave (PAW) formalism potential[22] using both generalized gradient approximation (GGA) PW91 (Ref. 23) functional and local density approximation (LDA) Ceperley–Alder functional[24] to explore the sensitivity of relative enthalpy to the functional form in the geometry optimization. All atomic positions and cell parameters are allowed to relax until the energy difference between geometry optimization steps is less than 1×10^{-6} eV per atom in contrast with Knight and Singer[9] who only optimized atomic positions but not the cell parameters. We adopted a Monkhorst–Pack[25] $2\times2\times2$ grid of *k*-points and a plane wave energy cutoff 520 eV to guarantee the convergence and the reliability of our simulation results. We increased the *k*-points grid up to $4\times4\times4$ in the DOS calculation with the tetrahedron method for better analyzing electronic structure.

The theoretical calculations of oxygen *K* edge XAS were based on DFT as implemented in the WIEN2K code,[26] which is very reliable when dealing with nanomaterials and crystals.[27] The final state was obtained by removing one 1*s* core electron to mimic the actual situation in XAS experiments. Using an atom with a reduced occupation in the core level within a supercell approximation has been a good and popular description for the calculation of core-level spectroscopy. Here, we used a supercell of 168 atoms. The missing full electron is replaced by an equally charged uniform background in our calculations using periodic boundary conditions. It is known that the choice of computational method

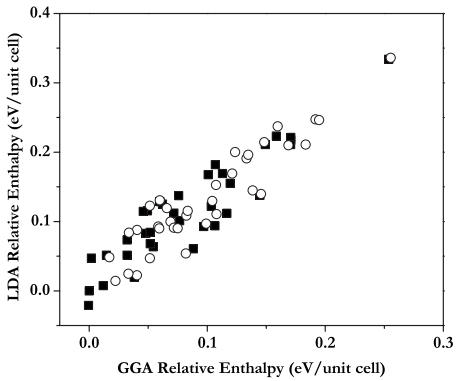

FIG. 1. Relative enthalpy (eV/unit cell) to the experimental ice XIII structure calculated by LDA and GGA of 70 selected structures. The solid squares and empty circles representing structures with space group P21/a and CC, respectively.

for studying XAS in water is a controversial issue so far.[15,20,28,29] In particular, half core hold (HCH) approach[30] has been shown to provide good agreement in the case of gas phase molecules and clusters[18,28,31] while full core ole (FCH), as in the present work, has been used in most applications to condensed phase systems.[20,32] In view of earlier results and discussions of FCH applied to water and ice,[15,20,29] we have carried out a systematic study of the dependence on unit cell size of the computed XAS spectra for ice Ih.[33] We obtained excellent agreement with experiment results using FCH for sufficiently large unit cell size (64 molecules) and good agreement, with all features reproduced semiquantitatively, for a 32 molecules cell; the HCH, on the other hand, does not reproduce the pre-edge and shoulder feature in the experiment. Hence, the unit cell of ice XIII contains 56 molecules which gives us confidence of a good agreement in the present case. For comparison with experiments, we have broadened the theoretical spectra with a Lorentzian of full width at half maximum=1.0 eV. In the calculation, we employed GGA PBE (Ref. 34) for exchange-correlation functional and we set $R^*_{mt}K_{\max}=5$ (where R_{mt} is the smallest atomic sphere radius in the unit cell and $K_{\max}$ is the magnitude of the largest *K* vector in the solution to the Kohn–Sham equation expansion $\psi_k=c_n\phi_{kn}$), which is sufficiently large for systems with hydrogen atoms. Calculated oxygen *K* edge XAS was obtained using Fermi golden rule and transition moments between a core electron and valence or conduction band state.[35] The absolute energy scale of the calculated DFT spectra was determined by shifting the spectra upward around 15 eV to coincide with the first excitation energy and the spectra lines were obtained by weight averaging on all distinct oxygen sites suggested by Limpijumnong *et al.*[36] It is important to note that our work concentrates on the shape of the core-level spectra (relative position of the peaks and spectral distributions) and does not attempt to determine the absolute threshold energy.

III. RESULTS AND DISCUSSIONS

The relative stability of these 70 selected high-symmetry structures at 0 GPa was depicted in Fig. 1. Here, we would like to estimate the contribution of zero point energy to the

total energy qualitatively. We found very small variation in the volume of the relaxed cells and the OH bond length variance is less than 0.0021 Å and the O–O variance is 0.024 Å. Consequently, the geometry of these configurations is almost identical, which indicates that the vibration modes (and hence the phonon sum and therefore the zero point energy) would be expected to be almost identical for each configuration. Therefore, it is safe to arrive at the conclusion that the contribution from the zero point energy is negligible between these closely related ice networks and the energy differences are principally dominated by the electrostatic interaction. The experimentally observed proton ordered structure is one of our DFT predicted lowest enthalpy configurations regardless of the exchange-correlation functional, which shows the energetic competitiveness and reliability of our methodology. We could see that these two space group symmetry structures scattered and mixed up together. In other words, no preference of low-enthalpy by LDA or GGA results was observed here. The overall trend in the stability is quite similar for LDA and GGA, even though the fitted line still deviates from the diagonal line; we attribute this minor discrepancy to the difference existing in LDA and GGA. Surprisingly, even LDA, which describes the water molecule geometry relatively poorly, gives similar results as the GGA functional. This implies that the exchange-correlation functional does not play an important role on the observed difference in total enthalpy. Therefore, by analysis of the DFT total energy expression we may speculate that differences in total enthalpy are due to the electrostatic interaction. From this, we can further deduce that the physical mechanism behind the proton ordering can be understood as a mainly electrostatic phenomenon as suggested by Tribello and Slater.[37]

From Fig. 1, however, we still can see some structures occasionally reverting in stability within these two exchange-correlation functionals, but there is a group of structures clearly lying near the true ground state. The small energetic difference makes it impossible to distinguish by DFT which one is the most stable structure. In the following, we chose four lowest-enthalpy (most stable) structures as displayed in Fig. 2 from the GGA results. It is known that the P21/a symmetry group has inversion symmetry and thus these four structures have no net dipole moment. The enthalpy difference between these four configurations is sufficiently small (less than 10^{-4} eV/water) that one would expect all these four configurations to be observed. In particular, configuration (a) has the same structure as the experimentally observed proton ordered structure.[1] We also double checked the relative enthalpy of these four structures with a larger k-point mesh ($3\times3\times3$) and higher plane wave cutoff (700 eV) in the optimization. All the evidences supported our prediction of energetic robustness of these four structures. Since cooling rate and strain[38] can affect the phase and the proportions of different phases, it is also reasonable that there exist lowest enthalpy configurations that are metastable forms of ice XIII, which are formed under kinetically controlled conditions. It has been shown recently that similar agreements with x-ray (XRD) and neutron diffraction data can be obtained with very different structures, including samples characterized by strongly distorted hydrogen bond networks.[39]

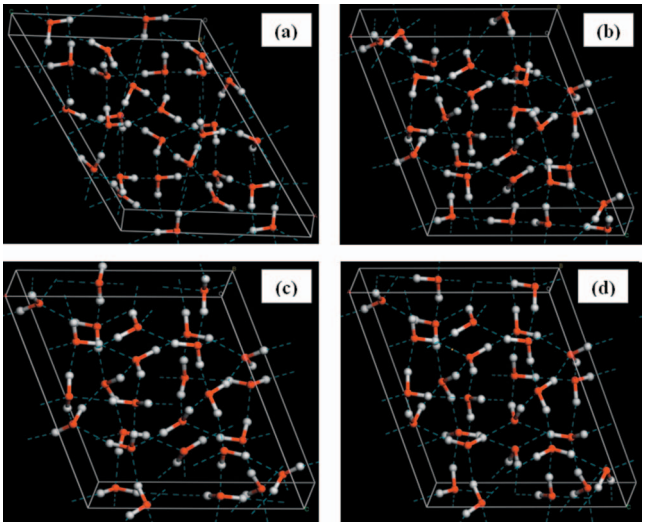

FIG. 2. Four predicted lowest enthalpy structures in which (a) is equivalent to the experimental structure in Ref. 1. The red and white balls represent oxygen and hydrogen atoms, respectively, and the light blue dashed lines represent hydrogen bonds.

Our calculated XRD and neutron diffraction data are given as supplemental material,[40] which shows that these two conventional structure determination methods are not distinguishable among these four structures. In the following, we will focus on this set of low-enthalpy structures and investigate their absorption features in the oxygen *K* edge XAS at ambient pressure with the purpose to provide helpful information on short range environments in these structures. Oxygen *K* edge XAS spectra with standard deviation obtained by averaging over different oxygen sites are plotted in Fig. 3. The pre-edge feature (~535 eV) was observed in all these four structures and when selectively exciting different oxygen atoms with minor differences between these four configurations. However, we can see that the standard deviation is very large in the main peak region (536–542 eV), which reflects a great sensitivity of this spectral region to the local chemical environment around oxygen atoms. Comparing these four configurations, the main spectra variances also lie in this main peak region. To summarize, this region offers the possibility to study the local environment of the absorbing oxygen atoms and does not require long range order, as necessary in XRD.

We also attempted to identify the origin of the different features in oxygen *K* edge XAS by comparing unbroadened angular momentum DOS, which is displayed in Fig. 4. We should note here that in order to compare with DOS, oxygen *K* edge XAS in Fig. 4 and Fig. 5 were not shifted and the Fermi level was indicated as 0. We could see that unbroadened DOS(p) of core holes contribute mainly to oxygen *K* edge XAS, as expected from the dipole selection rule. Since molecular orbital $4a_1$ has strong s character, we used DOS(s) to locate the $4a_1$ energy range. Obviously, DOS(s) has a very sharp peak at the pre-edge region. For the pre-edge, we could deduce that it mainly comes from O $1s$-$4a_1$ transitions while the main peak is mostly caused by O $1s$-$2b_2$ transitions. Furthermore, we probed effects of pressure on the oxygen *K* edge XAS. We carried out oxygen *K* edge XAS for structure

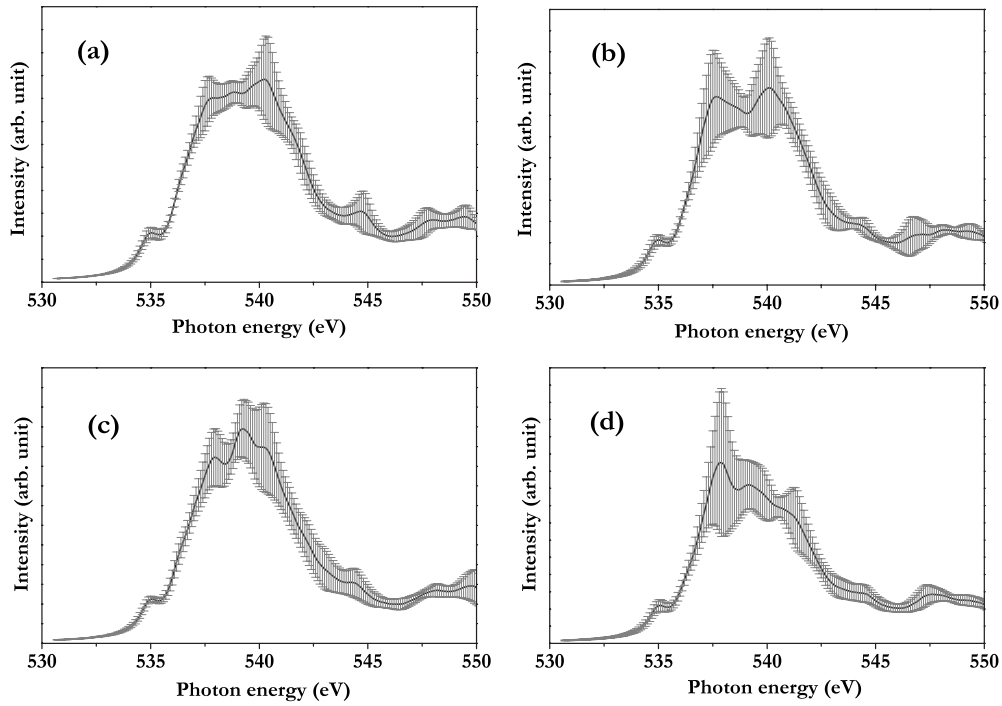

FIG. 3. Calculated oxygen *K* edge XAS of the corresponding four structures given in Fig. 2 with standard deviation obtained by averaging over all distinct oxygen sites.

(a) under 2 GPa. Obviously, the oxygen *K* edge XAS shifts to higher energy by ~1 eV compared to 0 GPa. This could be understood as the increased band gap (~0.9 eV) under compression. We can see that the pressure suppresses the pre-edge intensity. When pressure is applied to ice, the covalent OH bond would become longer and the hydrogen bond became shorter.[41] This is consistent with the explanations in which weakened hydrogen bonds may enhance pre-edge intensity.[16,18]

The total DOS and partial DOS (PDOS) of O 2*p* and H

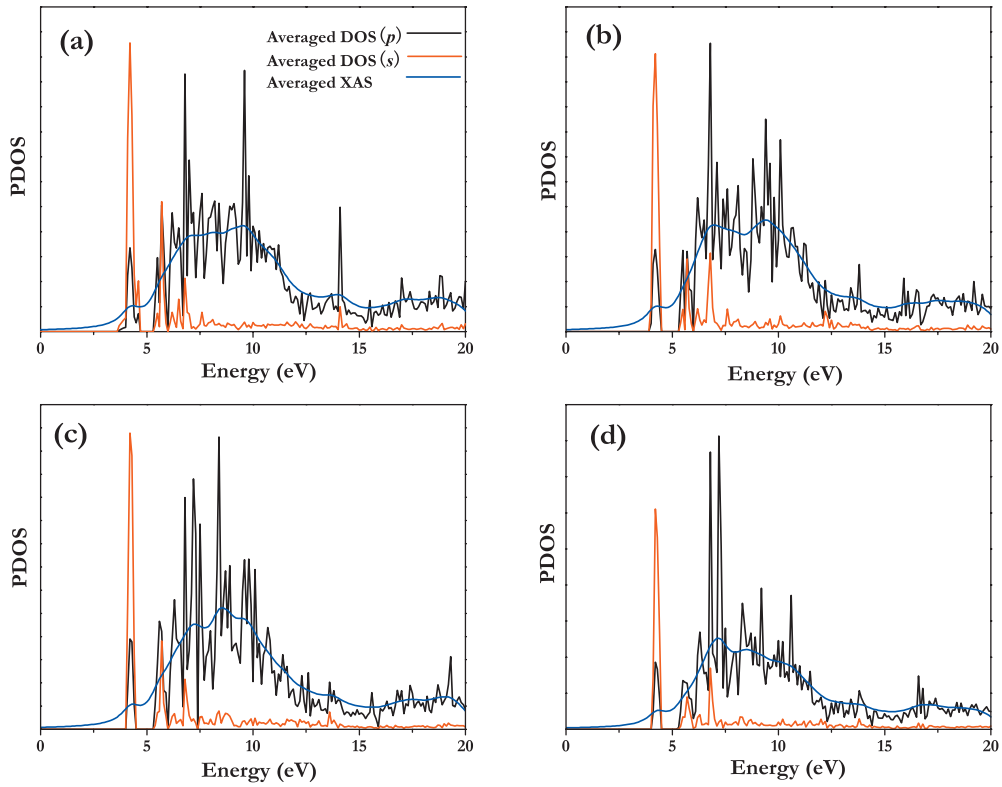

FIG. 4. Averaged PDOS of different oxygen core holes in four structures (DOS (*s*) in red line and DOS(*p*) in black line. Oxygen *K* edge XAS (in blue) are shown for comparison.

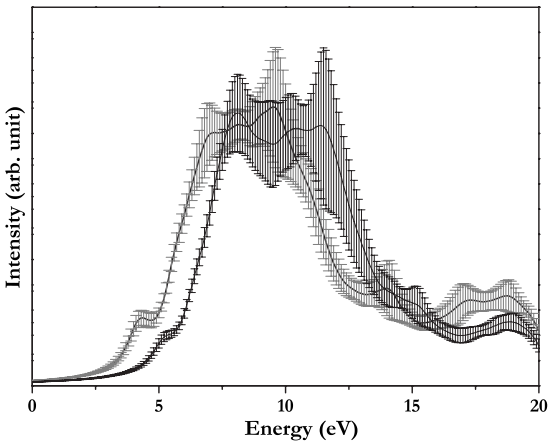

FIG. 5. Comparison of the calculated oxygen *K* edge XAS of structure (a) (shown in Fig. 2) under 0 GPa (gray) and 2 GPa (black).

1*s* electrons calculated for structure (a) under pressure are shown in Fig. 6. PDOS provides information of the atoms, which influences the electronic states through variation in the angular momentum of the states. The DOS near the Fermi level comes mainly from O 2*p* and partially from 1s in H. We do not chart O 1*s* as it shows a very small effect on the total DOS in comparison with O 2*p*. The fully occupied sets of bands consist of the overlapping bands of both O 2*p* and H 1*s* states, indicating a strong interaction between them. These bands are mainly responsible for the OH bond, exhibiting strong mixing. As for the total DOS, there is higher density at 0 GPa compared to higher pressure states near the Fermi level. The valence state of O can be obtained via distribution of O 2*p* electrons in the bonding $1b_2+3a_1$ bands which is occupied by the p_x, p_y, and p_z orbitals directly overlapping with the *s* orbital of the hydrogen and nonbonding $1b_1$ bands. Integration of each band of O 2*p* PDOS at 0 and

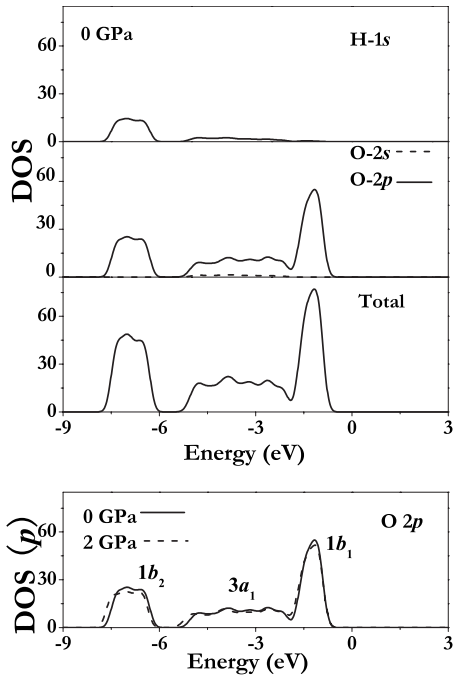

FIG. 6. Total DOS and PDOS for O 2*s*, O 2*p* electrons, and H 1*s* electrons of structure a at different pressures (0 and 2 GPa).

TABLE I. Integrated intensities of O 2*p* bands (electrons/unit cell) in structure (a) at different pressures.

Pressure (GPa)	$3a_1+1b_2$	$1b_1$
0	62.06	39.01
2	61.23	40.12

2 GPa is listed in Table I, where $1b_2+3a_1$ denotes the band from −8.16 to −1.81 eV and $1b_1$ shows the band from −1.81 to −0.20 eV for the 0 GPa case. As we can see from Table I, the integral intensity of the PDOS of the nonbonding $1b_1$ bands at 2 GPa is 1.11 higher than that at 0 GPa, or the participation of 2*p* electrons in the 2*p*-1*s* hybridization of O–H at 2 GPa is less than those at 0 GPa. In other words, the covalent OH bond becomes weaker at high pressure, which is also evidenced by the increasing OH bond length (as discussed above) due to the increased attraction of the proton by the accepting oxygen ion.[42] This could also be interpreted as a general trend of OH bond in water system under compression, as verified through more ionic OH bond in the ice VII/VIII transition under pressure, and finally transformed into symmetric hydrogen bond phase ice X, which is very similar to an ionic configuration.[43]

IV. CONCLUSIONS

In this work, we have used DFT to investigate hydrogen bond network, oxygen *K* edge XAS, and DOS in ice XIII under compression. We demonstrated that DFT methods have successfully reproduced the experimentally found structure. However, a few low-enthalpy metastable states are likely to coexist from the total enthalpy calculation results. This is reasonable due to the fact that the identity and concentration of dopants would probably influence the accessibility of these phases. We examined the applicability of oxygen *K* edge XAS to distinguish different hydrogen bond environments and found that the pre-edge is a common feature and the main spectral differences lie in the main peak region. By analyzing PDOS, the pre-edge feature of oxygen *K* edge XAS is identified to originate from O 1*s*-$4a_1$ transitions while the main peak is mostly caused by O 1*s*-$2b_2$ transitions. Under compression, the pre-edge intensity was suppressed which is due to the stronger hydrogen bond.

ACKNOWLEDGMENTS

We would like to thank Dr. T. Iitaka, Mr. Q. C. Nguyen, and Dr. X. F. Fan for helpful discussions. This work is financially supported by Academia Sinica, Nanyang Technological University, and the National Science Council of Taiwan (Grant No. NSC98-2113-M-001-029-MY3).

[1] C. G. Salzmann, P. G. Radaelli, A. Hallbrucker, E. Mayer, and J. L. Finney, Science **311**, 1758 (2006).
[2] J. L. Aragones, E. G. Noya, J. L. F. Abascal, and C. Vega, J. Chem. Phys. **127**, 154518 (2007); M. W. Mahoney and W. L. Jorgensen, *ibid.* **112**, 8910 (2000).
[3] E. Sanz, C. Vega, J. L. F. Abascal, and L. G. MacDowell, J. Chem. Phys. **121**, 1165 (2004).
[4] G. A. Tribello, B. Slater, and C. G. Salzmann, J. Am. Chem. Soc. **128**,

12594 (2006).
[5] D. R. Hamann, Phys. Rev. B **55**, R10157 (1997); D. D. Klug, J. S. Tse, Z. X. Liu, X. Gonze, and R. J. Hemley, *ibid.* **70**, 144113 (2004); J. S. Tse and D. D. Klug, Phys. Rev. Lett. **81**, 2466 (1998); K. Umemoto, R. M. Wentzcovitch, S. Baroni, and S. de Gironcoli, *ibid.* **92**, 105502 (2004).
[6] J. D. Bernal and R. H. Fowler, J. Chem. Phys. **1**, 515 (1933).
[7] M. Martin-Conde, L. G. MacDowell, and C. Vega, J. Chem. Phys. **125**, 116101 (2006).
[8] V. Buch, P. Sandler, and J. Sadlej, J. Phys. Chem. B **102**, 8641 (1998).
[9] C. Knight and S. J. Singer, J. Chem. Phys. **129**, 164513 (2008).
[10] C. Knight, S. J. Singer, J.-L. Kuo, T. K. Hirsch, L. Ojamae, and M. L. Klein, Phys. Rev. E **73**, 056113 (2006); J.-L. Kuo, J. V. Coe, S. J. Singer, Y. B. Band, and L. Ojamae, J. Chem. Phys. **114**, 2527 (2001).
[11] J.-L. Kuo, M. L. Klein, and W. F. Kuhs, J. Chem. Phys. **123**, 134505 (2005).
[12] J.-L. Kuo, Phys. Chem. Chem. Phys. **7**, 3733 (2005); J. L. Kuo and M. L. Klein, J. Phys. Chem. B **108**, 19634 (2004).
[13] J. L. Kuo and W. F. Kuhs, J. Phys. Chem. B **110**, 3697 (2006).
[14] J. Stöhr, *NEXAFS Spectroscopy* (Springer-Verlag, Berlin, 1992).
[15] D. Prendergast and G. Galli, Phys. Rev. Lett. **96**, 215502 (2006).
[16] S. Myneni, Y. Luo, L. A. Naslund, M. Cavalleri, L. Ojamae, H. Ogasawara, A. Pelmenschikov, P. Wernet, P. Vaterlein, C. Heske, Z. Hussain, L. G. M. Pettersson, and A. Nilsson, J. Phys.: Condens. Matter **14**, 106 (2002); P. Wernet, D. Nordlund, U. Bergmann, M. Cavalleri, M. Odelius, H. Ogasawara, L. A. Naslund, T. K. Hirsch, L. Ojamae, P. Glatzel, L. G. M. Pettersson, and A. Nilsson, Science **304**, 995 (2004).
[17] Y. Q. Cai, H. K. Mao, P. C. Chow, J. S. Tse, Y. Ma, S. Patchkovskii, J. F. Shu, V. Struzhkin, R. J. Hemley, H. Ishii, C. C. Chen, I. Jarrige, C. T. Chen, S. R. Shieh, E. P. Huang, and C. C. Kao, Phys. Rev. Lett. **94**, 025502 (2005); J. D. Smith, C. D. Cappa, K. R. Wilson, B. M. Messer, R. C. Cohen, and R. J. Saykally, Science **306**, 851 (2004).
[18] M. Cavalleri, H. Ogasawara, L. G. M. Pettersson, and A. Nilsson, Chem. Phys. Lett. **364**, 363 (2002).
[19] M. Odelius, M. Cavalleri, A. Nilsson, and L. G. M. Pettersson, Phys. Rev. B **73**, 024205 (2006); D. Nordlund, H. Ogasawara, P. Wernet, M. Nyberg, M. Odelius, L. G. M. Pettersson, and A. Nilsson, Chem. Phys. Lett. **395**, 161 (2004).
[20] B. Hetényi, F. De Angelis, P. Giannozzi, and R. Car, J. Chem. Phys. **120**, 8632 (2004).
[21] G. Kresse and J. Hafner, Phys. Rev. B **47**, 558 (1993).
[22] P. E. Blöchl, Phys. Rev. B **50**, 17953 (1994).
[23] J. P. Perdew, J. A. Chevary, S. H. Vosko, K. A. Jackson, M. R. Pederson, D. J. Singh, and C. Fiolhais, Phys. Rev. B **46**, 6671 (1992).
[24] D. M. Ceperley and B. J. Alder, Phys. Rev. Lett. **45**, 566 (1980).
[25] H. J. Monkhorst and J. D. Pack, Phys. Rev. B **13**, 5188 (1976).
[26] K. Schwarz, P. Blaha, and G. K. H. Madsen, Comput. Phys. Commun. **147**, 71 (2002).
[27] A. Titov, X. Biquard, D. Halley, S. Kuroda, E. Bellet-Amalric, H. Mariette, J. Cibert, A. E. Merad, G. Merad, M. B. Kanoun, E. Kulatov, and Y. A. Uspenskii, Phys. Rev. B **72**, 115209 (2005); C. L. Dong, C. Persson, L. Vayssieres, A. Augustsson, T. Schmitt, M. Mattesini, R. Ahuja, C. L. Chang, and J. H. Guo, *ibid.* **70**, 195325 (2004); J. H. Guo, L. Vayssieres, C. Persson, R. Ahuja, B. Johansson, and J. Nordgren, J. Phys.: Condens. Matter **14**, 6969 (2002).
[28] M. Odelius, J. Phys. Chem. A **113**, 8176 (2009); M. Cavalleri, M. Odelius, D. Nordlund, A. Nilsson, and L. G. M. Pettersson, Phys. Chem. Chem. Phys. **7**, 2854 (2005).
[29] R. L. C. Wang, H. J. Kreuzer, and M. Grunze, Phys. Chem. Chem. Phys. **8**, 4744 (2006).
[30] L. Triguero, L. G. M. Pettersson, and H. Agren, Phys. Rev. B **58**, 8097 (1998).
[31] M. Iannuzzi and J. Hutter, Phys. Chem. Chem. Phys. **9**, 1599 (2007).
[32] P. Rez, J. R. Alvarez, and C. Pickard, Ultramicroscopy **78**, 175 (1999); R. Buczko, G. Duscher, S. J. Pennycook, and S. T. Pantelides, Phys. Rev. Lett. **85**, 2168 (2000); K. Lie, R. Hoier, and R. Brydson, Phys. Rev. B **61**, 1786 (2000); C. Elsässer and S. Kostlmeier, Ultramicroscopy **86**, 325 (2001); I. Tanaka, H. Araki, M. Yoshiya, T. Mizoguchi, K. Ogasawara, and H. Adachi, Phys. Rev. B **60**, 4944 (1999).
[33] J. Zhang, Z. R. Xiao, and J. L. Kuo, "The supercell consist of 32 molecules of ice Ih following the same procedures described here" (to be published).
[34] J. P. Perdew, K. Burke, and M. Ernzerhof, Phys. Rev. Lett. **77**, 3865 (1996).
[35] K. Schwarz, A. Neckel, and J. Nordgren, J. Phys. F: Met. Phys. **9**, 2509 (1979); K. Schwarz and E. Wimmer, *ibid.* **10**, 1001 (1980).
[36] S. Limpijumnong, S. Rujirawat, A. Boonchun, M. F. Smith, and B. Cherdhirunkorn, Appl. Phys. Lett. **90**, 103113 (2007); J. T-Thienprasert, J. Nukeaw, A. Sungthong, S. Porntheeraphat, S. Singkarat, D. Onkaw, S. Rujirawat, and S. Limpijumnong, *ibid.* **93**, 051903 (2008).
[37] G. A. Tribello and B. Slater, Chem. Phys. Lett. **425**, 246 (2006).
[38] C. M. B. Line and R. W. Whitworth, J. Chem. Phys. **104**, 10008 (1996).
[39] A. K. Soper, J. Phys.: Condens. Matter **17**, S3273 (2005); M. Leetmaa, K. T. Wikfeldt, M. P. Ljungberg, M. Odelius, J. Swenson, A. Nilsson, and L. G. M. Pettersson, J. Chem. Phys. **129**, 084502 (2008); K. T. Wikfeldt, M. Leetmaa, M. P. Ljungberg, A. Nilsson, and L. G. M. Pettersson, J. Phys. Chem. B **113**, 6246 (2009); M. Iannuzzi, J. Chem. Phys. **128**, 204506 (2008).
[40] See supplementary material at http://dx.doi.org/10.1063/1.3421650 for simulated XRD and neutron diffraction data of four structures shown in Fig. 2.
[41] M. Benoit and D. Marx, ChemPhysChem **6**, 1738 (2005); M. Benoit, D. Marx, and M. Parrinello, Nature (London) **392**, 258 (1998).
[42] W. L. Vos, L. W. Finger, R. J. Hemley, and H. K. Mao, Chem. Phys. Lett. **257**, 524 (1996).
[43] R. Caracas, Phys. Rev. Lett. **101**, 085502 (2008).